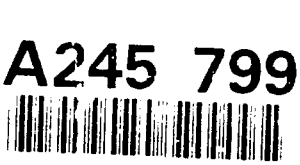

NPS ME-92-001

NAVAL POSTGRADUATE SCHOOL

Monterey, California

STRESSES IN SOLDER JOINTS OF ELECTRONIC PACKAGES

by

DAVID SALINAS

and

PHILIP Y. SHIN

December 1991

Prepared for:
Naval Weapons Support Center
Code 0211
Crane Indiana 47522

Naval Postgraduate School
Monterey, California

Rear Admiral R. W. West, Jr.
Superintendent

H. Shull
Provost

This report was prepared for and funded by the Naval Weapons Support Center, Code 0211, Crane Indiana, 47522.

This report was prepared by:

David Salinas
DAVID SALINAS
Assoc. Prof. of Mech. Engn'g.

PHILIP Y. SHIN
Asst. Prof. of Mech. Engn'g.

Reviewed by:

ANTHONY J. HEALEY
Chairman, Dept. of Mech. Engn'g.

Released by:

PAUL J. MARTO
Dean of Reasearch

SECURITY CLASSIFICATION OF THIS PAGE

REPORT DOCUMENTATION PAGE

1a REPORT SECURITY CLASSIFICATION: UNCLASSIFIED	1b RESTRICTIVE MARKINGS
2a SECURITY CLASSIFICATION AUTHORITY	3 DISTRIBUTION/AVAILABILITY OF REPORT: APPROVED FOR PUBLIC RELEASE: UNLIMITED DISTRIBUTION
2b DECLASSIFICATION/DOWNGRADING SCHEDULE	
4 PERFORMING ORGANIZATION REPORT NUMBER(S): NPS ME-92-001	5 MONITORING ORGANIZATION REPORT NUMBER(S)
6a NAME OF PERFORMING ORGANIZATION: DEPT. OF MECH. ENGN'G. / 6b OFFICE SYMBOL (If applicable): ME	7a NAME OF MONITORING ORGANIZATION
6c ADDRESS (City, State, and ZIP Code): NAVAL POSTGRADUATE SCHOOL, MONTEREY, CA 93943-5100	7b ADDRESS (City, State, and ZIP Code)
8a NAME OF FUNDING SPONSORING ORGANIZATION: NAVAL WEAPONS SUPPORT CTR. / 8b OFFICE SYMBOL (If applicable)	9 PROCUREMENT INSTRUMENT IDENTIFICATION NUMBER: N0003091WR12709
8c ADDRESS (City, State, and ZIP Code): CRANE, INDIANA 47522	10 SOURCE OF FUNDING NUMBERS: PROGRAM ELEMENT NO / PROJECT NO / TASK NO / WORK UNIT ACCESSION NO

11 TITLE (Include Security Classification): STRESSES IN SOLDER JOINTS OF ELECTRONIC PACKAGES (UNCL.)

12 PERSONAL AUTHOR(S): DAVID SALINAS AND PHILIP Y. SHIN

13a TYPE OF REPORT	13b TIME COVERED	14 DATE OF REPORT (Year, Month, Day)	15 PAGE COUNT
FINAL REPORT	FROM JAN 91 TO SEP 91	1991 DEC 31	27

16 SUPPLEMENTARY NOTATION

17 COSATI CODES			18 SUBJECT TERMS (Continue on reverse if necessary and identify by block number)
FIELD	GROUP	SUB-GROUP	THERMOELASTIC STRESSES, ELECTRONIC PACKAGES

19 ABSTRACT (Continue on reverse if necessary and identify by block number)

An investigation of stresses, arising from a thermal field, in electronic packages comprised of ceramic chip and composite board attached by a solder adhesive joint was undertaken. Two types of solder joints, a leaded device and an unleaded device, were compared for effectiveness. Procedures are shown for the analyses of these two types of solder joints. The analyses showed that the thermoelastic stresses for the stiff unleaded connection are significantly greater, by a factor of 20 for the particular arrangement studied in this report, than the stresses in the more flexible leaded connection.

20 DISTRIBUTION/AVAILABILITY OF ABSTRACT	21 ABSTRACT SECURITY CLASSIFICATION
☒ UNCLASSIFIED/UNLIMITED ☐ SAME AS RPT ☐ DTIC USERS	

22a NAME OF RESPONSIBLE INDIVIDUAL	22b TELEPHONE (Include Area Code)	22c OFFICE SYMBOL
Prof. David Salinas	(408) 646-3426	ME/Sa

DD FORM 1473, 84 MAR — 83 APR edition may be used until exhausted. All other editions are obsolete.

SECURITY CLASSIFICATION OF THIS PAGE

☆ U.S. Government Printing Office: 1986—606-24

ABSTRACT

An investigation of stresses, arising from a thermal field, in electronic packages comprised of a ceramic chip attached to a composite board by a solder joint was undertaken. Two types of solder joint connections, a leaded device and an unleaded device, were analyzed. The stresses result from the mismatch of material properties of the tri-assembly system. Procedures are shown for the analyses of the two types of solder connections. The analyses showed that the thermoelastic stresses for the stiff unleaded connection are significantly greater, by a factor of 20 for a the particular application undertaken in this report, than the thermoelastic stresses in the flexible leaded connection.

Introduction

Electronic chip packages are comprised of several components with different material properties and geometries. One of the most basic electronic packages is the tri-assembly system consisting of a chip attached to a board by a solder connection. During the fabrication of this simple unit, the soldering process subjects the device to a thermal field. Since the three components of the device have different material properties, in particular their Young's modulii, Poissons ratios, and thermal coefficients of expansion, the mismatch in these properties result in thermoelastic stresses. In addition to the thermal field arising from fabrication, thermal fields and hence thermoelastic stresses, result from the operation of the device itself.

Not only is the mismatch in material properties important in the thermoelastic stresses that develop, but equally important is the manner in which the solder connection is made. For a given set of chip, board and solder properties, an important question 'what is the best way to make the solder connection?'. With regard to geometric configuration, there are two main types of connections, the leaded connection and the unleaded connection. In the leaded connection, the chip is attached to the board by a thin 'lead' as shown in Figure 1. In this configuration, the chip is somewhat removed from the board its attached to. In contrast, in the unleaded connection, the chip is attached along its edges to the board substrate by a thin layer of solder. This unleaded joint arrangement is significantly 'stiffer' than the leaded connection, and all other things being equal, one would expect that the stiffer unleaded joint would result in larger thermoelastic stresses. This investigation seeks to determine the relative magnitudes of the stresses from these two kinds of solder joints. It should be noted however, that the proximity of the chip to the board, in the unleaded joint, might result in a more uniform thermal field thereby reducing the thermal gradients and thus the thermal stresses. The question of the thermal field that results from each of the solder joints is not addressed in this investigation which only considers the effect of the same uniform thermal environment on each of these (leaded and unleaded) solder joints.

Analysis of leaded device

Figure 1 shows the geometry and dimensions of the leaded device considered in this study which consists of a ceramic chip, lead wires and a circuit board. The cross-sectional dimension of the lead wire is given in Figure 2.

Three general assumptions are made. First, the whole device is under a thermal cycling load of +65°c ~ -20°c and the lead wire has an initial strain from soldering process. The device is soldered to the circuit board at a temperature of +185°c and this tempature is assumed to propagate only to the lead wire during the soldering. Another assumption is on the deformation of the device that the ceramic chip and the circuit board are so much stiffer than the leads so all the deflections due to the thermal loading occur only to the leads. Finally, the device is assumed to be geometrically symmetric about the center so the following calculation is performed only for the half of the device.

Material properties of the chip, lead and the glass-epoxy substrate of the circuit board are as follows;

Thermal expansion factor of the chip, $\alpha_c = 6.5\ 10^{-6}$ ppm/°c
Thermal expansion factor of the lead, $\alpha_L = 4.47\ 10^{-6}$ ppm/°c
Thermal expansion factor of the substrate, $\alpha_s = 16.\ 10^{-6}$ ppm/°c

Young's modulus of the lead wire, $E = 21.\ 10^6$ psi
Moments of inertia of the lead wire, $I = bh^3/12 = 0.017\ (0.005)^3/12 = 1.77\ 10^{-10}$ in^4

Calculation of thermal mismatch

At +20°c;

Initial deformation of a lead wire after the welding (from +185 c to +20 c)

$\Delta_{INIT} = \alpha\ \Delta T(L) = 4.47\ 10^{-6}(-165\ c)(0.045) = -33.2\ 10^{-6}$ in

At +65°c;

Deformations due to temperature changes from +20°c to +65°c

$\Delta_{chip} = \alpha_c \Delta T(L_c) = 6.5\ 10^{-6}(45°c)(0.26/2) = 38.0\ 10^{-6}$ in
$\Delta_{lead} = \alpha_L \Delta T(L_L) = 4.47\ 10^{-6}(45°c)(0.045) = 9.1\ 10^{-6}$ in
$\Delta_{sub} = \alpha_s \Delta T(L_s) = 16.\ 10^{-6}(45°c)(0.35/2) = 126.0\ 10^{-6}$ in

Mismatch between the top(chip and lead) and the bottom portion(substrate) is

$\Delta_{65°} = \Delta_{top} - \Delta_{bot}$
$= (\Delta_{chip} + \Delta_{lead} + \Delta_{INIT}) - (\Delta_{sub})$
$= (38.0\ 10^{-6} + 9.1\ 10^{-6} - 33.2\ 10^{-6}) - (126.0\ 10^{-6})$
$= -112.1\ 10^{-6}$ in

At -20°c;

Deformations due to temperature changes from +20°c to -20°c

$\Delta_{chip} = \alpha_c \Delta T(L_c) = 6.5\ 10^{-6}(-40°c)(0.26/2) = -33.8\ 10^{-6}$ in
$\Delta_{lead} = \alpha_L \Delta T(L_L) = 4.47\ 10^{-6}(-40°c)(0.045) = -8.05\ 10^{-6}$ in
$\Delta_{sub} = \alpha_s \Delta T(L_s) = 16.\ 10^{-6}(-40°c)(0.35/2) = -112.\ 10^{-6}$ in

Mismatch between the top(chip and lead) and the bottom portion(substrate) is

$\Delta_{-20°} = \Delta_{top} - \Delta_{bot}$
$= (\Delta_{chip} + \Delta_{lead} + \Delta_{INIT}) - (\Delta_{sub})$
$= (-33.8\ 10^{-6}\ -8.1\ 10^{-6} - 33.2\ 10^{-6}) - (-112.\ 10^{-6})$
$= 36.9\ 10^{-6}$ in

Since $\Delta_{65°}$ is much greater than $\Delta_{-20°}$ in its magnitude, it is considered that $\Delta_{65°}$ becomes critical for the stress calculation.

Analogy of temperature change effect and support settlement effect

It can be seen that the force balance from the temperature

changes are the same as that from the support settlement shown in Figure 3. So we now treat the displacement Δ_{65° from the above calculation as the settlement δ.

$$\delta = \Delta_{65^\circ}$$

To find the force P cause by a displacement δ which is known from the previous calculation, we'll break the frame ABC into beam AB and beam BC as in Figure 4 and 5.

Denoting L_v and L_h as the length of the beam AB and BC, respectively, the tip displacements and the tip rotations at the beam AB due to an applied force P_B and a moment M_B are given by the formulas

$$\delta = \frac{PL_v^3}{3EI} - \frac{ML_v^2}{2EI} \tag{1}$$

$$\theta_B = \frac{PL_v^2}{2EI} - \frac{ML_v}{EI} \tag{2}$$

and for beam BC the tip rotations can be expressed by

$$\theta_B = \frac{ML_h}{EI} \tag{3}$$

Compatibility requires that θ_B at the above equations (2) and (3) be the same so by equating these two equations an expression for M can be found.

$$M = \frac{PL_v^2}{2(L_v + L_h)} \tag{4}$$

Substituting (4) into (1)

$$\delta = \frac{PL_v^3}{EI} \frac{L_v + 4L_h}{12(L_v + L_h)}$$

or P can be written in terms of δ,

$$P = \frac{\delta EI}{L_v^3} \frac{12(L_v + L_h)}{L_v + 4L_h}$$

$$= \frac{112.1\ 10^{-6}\ (21.\ 10^6)\ (1.77\ 10^{-6})}{(0.028)^3} \frac{12(0.028 + 0.045)}{0.028 + 4(0.045)} = 0.0811\ \text{lb}$$

Shear stress calculation

The shear stresses at the solder joint are obtained by dividing the force by footage area of the lead wire which is soldered to the circuit board,

$$\tau = \frac{P}{A} = \frac{P}{bL} = \frac{0.0811}{0.017(0.03)} = \mathbf{159.0\ psi}$$

Analysis of unleaded device

Figure 6 shows the geometry and dimensions of the unleaded device which consists of a ceramic chip fixed to a circuit board by a thin strip of solder. In the present application, the solder adhesive layer covers only a small area along the edge of the chip.

Two models of the problem follows. The first model, developed by Suhir (1), provides an analytical determination of thermally-induced stresses in a tri-material assembly. The second model is a finite element model which utilizes a recently developed element which maintains inter-layer continuity along the chip-solder and board-solder interfaces.

Suhir's Model

A free body diagram of the tri-material assembly, showing the notation used hereafter, is shown in Figure 7. The Suhir model is applicable to assemblies with continuous attachment (a = l), as well as non-continuous attachment (a < l). The development is carried through by invoking equilibrium, displacement compatibility, and thermoelastic constitutive relations. The displacement compatibility relations impose the condition of inter-layer displacement continuity. For a detailed development of the analytical relations, the reader is referred to the original work. Here a brief summary of the development is presented, followed by a sequential list of the calculations that lead to the maximum interlayer shearing stress.

Denoting the axial displacements at the top and bottom of the i^{th} layer as $u^+_i(x) = u^-_i(x)$ respectively, the displacement compatibility conditions along the interfaces of layers 1-2 and layers 2-3 are:

$$u_1^-(x) = u_2^+(x) \qquad (5)$$

$$u_2^-(x) = u_3^+(x) \qquad (6)$$

Axial displacements $u^-_1(x)$, $u^+_2(x)$, $u^-_2(x)$, and $u^+_3(x)$ are obtained by adding the individual contributions to these displacements arising from (a) thermal expansion, (b) axial forces, (c) shear forces, and (d) bending moments. The moments are related to the axial forces by the moment equilibrium equation which gives

$$\frac{h_1 + h_2}{2} T_1(x) + \frac{h_2 + h_3}{2} T_2(x) = M_1 + M_2 + M_3 \qquad (7)$$

where T_1 and T_2 are the axial forces on layers 1 and 2. The T_i axial forces are related through equilibrium to the shear stresses between layers, that is

$$T_i(x) = \int_{-1}^{x} \tau_i(\xi)\, d\xi \qquad (8)$$

where $\tau_i(x)$ is the shear stress between the i^{th} and $(i + 1)^{st}$ layers. The M_i moments are related to the radii of curvature, ρ_i through

$$M_i(x) = - \frac{D_i}{\rho(x)} \qquad i = 1,2,3 \qquad (9)$$

and the D_i flexural rigidity coefficients for each layer are given by

$$D_i = \frac{E_i h_i^3}{12(1 - \nu_i^2)} \qquad (10)$$

where E_i, h_i, and ν_i are the Young's modulus, thickness, and Poisson's ratio of the i^{th} layer respectively. Equation (10) assumes there is no variation of lateral displacement with respect to y, and therefore the radii of curvature of layers are all equal.

Using equilibrium equation (7) and moment-curvature equation (9) yields

$$\frac{1}{\rho(x)} = -T_1(x) \sqrt{\frac{\lambda_{12}}{D}} - T_3(x) \sqrt{\frac{\lambda_{23}}{D}} \qquad (11)$$

where

$$D = D_1 + D_2 + D_3 \qquad (12)$$

is the flexural rigidity of the assembly, and where

$$\lambda_{i,i+1} = \frac{(h_i + h_{i+1})^2}{2D} \qquad (13)$$

is an additional compliance due to bowing. The individual contributions to Eqn's (5) and (6) are the

- the thermal contribution is:

$$\alpha_i (\Delta T)_i x \tag{14}$$

- the axial force contribution is:

$$-\lambda_i \int_0^x T_i(\xi)\, d\xi \tag{15}$$

where λ_i is the axial compliance of the i^{th} layer, given by

$$\lambda_i = \frac{1-\nu_i}{E_i h_i} \tag{16}$$

- the shear stress contribution is: $-\kappa_i \tau_i(x)$, where κ_i is the interfacial compliance given by

$$\kappa_i = \frac{h_i}{3G_i} \tag{17}$$

- the rotational contribution is:

$$\frac{-h_i}{2} \int_0^x \frac{d\xi}{\rho(\xi)} \tag{18}$$

Invoking the condition that the shear stresses be anti-symmetric with respect to the origin of coordinates leads to the expression

$$\tau_i(x) = C_i \sinh kx \qquad i=1,2 \tag{19}$$

where k is obtained by solving a characteristic equation defined in Eq.(20) below. Substitution of the above expressions into compatibility conditions (5) and (6) yields the quartic equation

$$\kappa_{12}\kappa_{33} k^4 - (\kappa_{12}\lambda^{\circ}_{23} + \kappa_{23}\lambda^{\circ}_{12})\, k^2 + \delta = 0 \tag{20}$$

where the κ_{ij}'s and λ_{ij}'s are interfacial and axial compliances, respectively, of the tri-material assembly, given by

$$\kappa_{12} = \kappa_1 + \kappa_2 \tag{21}$$

$$\kappa_{23} = \kappa_2 + \kappa_3 \tag{22}$$

$$\lambda_{23}^{0} = \lambda_2 + \lambda_3 + \lambda_{23} \tag{23}$$

$$\lambda_{12}^{0} = \lambda_1 + \lambda_2 + \lambda_{12} \tag{24}$$

$$\delta = \lambda_1\lambda_2 + \lambda_2\lambda_3 + \lambda_3\lambda_1 + \lambda_3\lambda_{12} + \lambda_2(\sqrt{\lambda_{12}} + \sqrt{\lambda_{23}})^2 \tag{25}$$

Letting $\omega = k^2$, Eq.(20) becomes

$$\kappa_{12}\kappa_{33}\omega^2 - (\kappa_{12}\lambda_{23}^{0} + \kappa_{23}\lambda_{12}^{0})\omega + \delta = 0 \tag{26}$$

whose solution is

$$\omega_{1,2} = \frac{-b \pm \sqrt{b^2 - 4ac}}{2a} \tag{27}$$

where

$$a = \kappa_{12}\kappa_{33} \qquad b = -(\kappa_{12}\lambda_{23}^{0} + \kappa_{23}\lambda_{12}^{0}) \tag{28}$$

The k_i $(i=1,2)$ roots are then obtained as

$$k_{1,2} = \pm\sqrt{\omega_1} \qquad k_{3,4} = \pm\sqrt{\omega_2} \tag{29}$$

The expressions presented above, valid for any tri-material assembly, reduce to the simpler form

$$\tau(x) = k\frac{\Delta\alpha\,\Delta t}{\lambda \cosh kl}\sinh kx \tag{30}$$

where

$$k = \sqrt{\frac{\lambda_{23}^{0}}{\kappa}} \qquad \kappa = \kappa_1 + 2\kappa_2 + \kappa_3 \tag{31}$$

when the Youngs modulus of the mid layer, or its thickness is very small, as in the case of a thin layer of solder used as an adhesive. In accordance with Eq.(19), the maximum shear stress occurs at $x = \ell$, and can be calculated from
where

$$\tau_{max} = k\frac{\Delta\alpha\,\Delta T}{\lambda}\chi_{max} \qquad (32)$$

$$\chi_{max} = 1 - \frac{\cosh k(l-a)}{\cosh kl} \qquad (33)$$

Application of Suhir Model to Unleaded Device

Here, the closed form equations from Suhir's model are used to determine the shear stresses in an uleaded device. The application is to unleaded device with dimensions and material properties as follows:

Material #1; Ceramic chip:

α_1 = 3.6x10^{-6} in/in/F, ν = 0.3, E_1 = 40x10^6 psi,
G_1 = 15.4x10^6 psi, h_1 = .056 in.

Material #2; Solder:

α_1 = 25.x10^{-6} in/in/F, ν = 0.3, E_2 = 1.86x10^6 psi,
G_2 = .66x10^6 psi, h_2 = .002 in.

Material #3; (board):

α_3 = 16.x10^{-6} in/in/F, ν = 0.4, E_3 = 2.0x10^6 psi
G_3 = .77x10^6 psi, h_3 = .056 in.

The above parameters lead to the following compliances:

Chip: D_1 = 643 lb.in., λ_1 = .3125x10^{-6} in./lb.,
κ_1 = 1.212x10^{-9} in./lb.

Solder: D_2 = .0231 lb.in., λ_2 = 64.52x10^{-6} in./lb.,
κ_2 = 2.525x10^{-9} in./lb.

Board: D_3 = 32.2 lb.in., λ_3 = 6.25x10^{-6} in./lb.,
κ_3 = 24.24x10^{-9} in./lb.

The other parameter values necessary for a solution are:

$\lambda_{1,2}$ = 1.378x10^{-6} in./lb. $\lambda_{2,3}$ = 1.378x10^{-6} in./lb.

$\kappa_{1,2} = 3.737 \times 10^{-9}$ in./lb. $\quad\quad$ $\kappa_{2,3} = 26.77 \times 10^{-9}$ in./lb.

$\lambda_{12}' = 64.83 \times 10^{-6}$ in./lb. $\quad\quad$ $\lambda_{23}' = 70.77 \times 10^{-6}$ in./lb.

$\lambda_{12}^{0} = 66.21 \times 10^{-6}$ in./lb. $\quad\quad$ $\lambda_{23}^{0} = 72.15 \times 10^{-6}$ in./lb.

Substitution of these parameters into Eq.(25) yields

$$\delta = .7897 \times 10^{-9} \text{ (in./lb.)}^2$$

which upon substitution into Eq.(26) yields $k = 19.85$ in.$^{-1}$. Finally, the maximum shear stress at the solder interface is obtained from Eq.(32) as

$$\tau_{max} = \mathbf{4360 \text{ psi}}$$

The simpler approximate expression for k from Eq.(31) yields k = 19.61 in.$^{-1}$, which, in turn, gives τ_{max} = 4310 psi.

Finite Element Model

An alternate model of the tri-assembly problem using a finite element method was undertaken. Continuity along the interfaces of adjacent layers is maintained by selection of the six degree of freedom element shown in Figure 8. The six degrees of freedom are as follows:

δ_1 is the axial displacement at the lower left corner

δ_2 is the axial displacement at the upper right corner

δ_3 is the lateral displacement at the left end

δ_4 is the axial displacement at the lower right corner

δ_5 is the axial displacement at the upper right corner

δ_6 is the lateral displacement at the right end

The axial displacement field u(x,y) is taken as linear interpolation in both the axial, x, and transverse, y, directions. That is,

$$u(x,y) = H_1(y)\,(N_1(x)\,\delta_1 + N_2(x)\,\delta_2) + H_2(y)\,(N_1(x)\,\delta_4 + N_2(x)\,\delta_5) \quad (34)$$

and the lateral (i.e.,transverse) displacement field is a linear function of x, that is,

$$v(x) = N_1(x)\,\delta_3 + N_2(x)\,\delta_6 \tag{35}$$

where the linear interpolation functions are:

$$H_1(y) = \frac{1}{h}(h-y) \tag{36}$$

$$H_2(y) = \frac{y}{h} \tag{37}$$

$$N_1(x) = \frac{1}{l}(l-x) \tag{38}$$

$$N_2(x) = \frac{x}{l} \tag{39}$$

The strain-displacement relations are:

$$\epsilon_x = \frac{\partial u}{\partial x} = \frac{H_1(y)}{l}(\delta_4-\delta_1) + \frac{H_2(y)}{l}(\delta_5-\delta_2) \tag{40}$$

$$\gamma_{xy} = \frac{\partial u}{\partial y} + \frac{\partial v}{\partial x} = \frac{N_1(x)}{h}(\delta_2-\delta_1) + \frac{N_2(x)}{h}(\delta_5-\delta_4) + \frac{\delta_6-\delta_3}{l} \tag{41}$$

On the element level, we have the bending effects

$$K_B\delta_B = F_B \tag{42}$$

where

$$\delta_B^T = \langle \delta_1 \quad \delta_2 \quad \delta_4 \quad \delta_5 \rangle \tag{43}$$

and

$$K_B = \int_0^l \int_0^h BEB^T dydx \tag{44}$$

and

$$B^T = \langle \frac{\partial N_1}{\partial x} H_1 \quad \frac{\partial N_1}{\partial x} H_2 \quad \frac{\partial N_2}{\partial x} H_1 \quad \frac{\partial N_2}{\partial x} H_2 \rangle \tag{45}$$

and

$$F_B = \int_0^l \int_0^h B E B^T dy\, dx \tag{46}$$

which gives

$$K_B = \frac{Eh}{6l} \begin{bmatrix} 2 & 1 & -2 & -1 \\ 1 & 2 & -1 & -2 \\ -2 & -1 & 2 & 1 \\ 1 & -2 & 1 & 2 \end{bmatrix} \tag{47}$$

Similarly for the shear effects

$$K_S \delta_S = 0 \tag{48}$$

where

$$\delta_S^T = \langle \delta_1 \quad \delta_2 \quad \delta_3 \quad \delta_4 \quad \delta_5 \quad \delta_6 \rangle \tag{49}$$

and

$$K_S = \int_0^l \int_0^h B' G B'^T dy\, dx \tag{50}$$

where

$$B'^T = \langle N_1 \frac{\partial H_1}{\partial y} \quad N_1 \frac{\partial H_2}{\partial y} \quad \frac{\partial N_1}{\partial x} \quad N_2 \frac{\partial H_1}{\partial y} \quad N_2 \frac{\partial H_2}{\partial y} \quad \frac{\partial N_2}{\partial x} \rangle \tag{51}$$

which gives

$$K_S = \begin{bmatrix} a & -a & \frac{G}{2} & a & -a & \frac{G}{2} \\ -a & a & -\frac{G}{2} & -a & a & \frac{G}{2} \\ \frac{G}{2} & -\frac{G}{2} & b & \frac{G}{2} & -\frac{G}{2} & -b \\ a & -a & \frac{G}{2} & a & -a & -\frac{G}{2} \\ -a & a & -\frac{G}{2} & -a & a & \frac{G}{2} \\ -\frac{G}{2} & \frac{G}{2} & -b & -\frac{G}{2} & \frac{G}{2} & b \end{bmatrix} \qquad (52)$$

The bending and shear element stiffness matrices are combined to form the element stiffness matrix, which in turn are again combined to form the system stiffness matrix. In accordance with standard FEM techniques, the system matrix equations are solved for the system displacement degrees of freedom. The element strains are then calculated from Eq.(40) and (41) above. Finally, the average bending stresses at the bottom and top of an element are obtained from the stress-strain relations

$$(\sigma_x)_1 = \frac{\delta_4 - \delta_2}{l} \qquad (53)$$

and

$$(\sigma_x)_2 = \frac{\delta_5 - \delta_2}{l} \qquad (54)$$

Similarly, the average element shear stresses are calculated from the strress-strain relations

$$(\tau_{xy})_1 = G\left(\frac{\delta_2 - \delta_1}{h} + \frac{\delta_6 - \delta_3}{l}\right) \qquad (55)$$

and

$$(\tau_{xy})_2 = G\left(\frac{\delta_5 - \delta_4}{h} + \frac{\delta_6 - \delta_3}{l}\right) \qquad (56)$$

The finite element mesh, shown in Figure 9, consisting of 104 elements and 149 degrees of freedom produced an interface maximum shear stress of 3650 psi. This FEM calculated stress is at the midpoint of the right most element. This stress, obtained from an FEM analysis is at the midpoint of the interface at the right most element. Quadratic extrapolation to approximate the hyperbolic sine expression for the τ shear stress brings the FEM predicted value to about **3800** psi. Thus the predicted values of the maximum shear stress from the Suhir model and the FEM model differ by less than 15 percent.

Conclusions

This investigation has shown that under the same thermal environment, the stiff unleaded solder joint has significantly higher thermoelastic stresses than the flexible leaded solder joint. Since the unleaded joint has a stronger suppression of displacement than the leaded joint, and thermal stresses result from displacement constraint, the result is not an unexpected one. In the particular application presented in the previous sections, the stresses in the unleaded connection were twenty times the stresses in the leaded connection. This large degree of difference between the stresses in the two cases is surprising.

As previously noted, the comparison is for the case where both connections are subjected to the same thermal environment. This assumption does not take into account the fact that the thermal field is very likely to be different for the two types of joints. One might expect that the leaded joint with the 'separated' components may have larger thermal gradients than the unleaded joint where the components are in close proximity to each other and therefore may have a more uniform thermal field. In fact, the solution to the stress problem really requires its coupling to the thermal (energy balance) problem. This later coupled (and transient) problem is presently under investigation as a NPS thesis topic under the direction of D. Salinas and Y.W. Kwon (2).

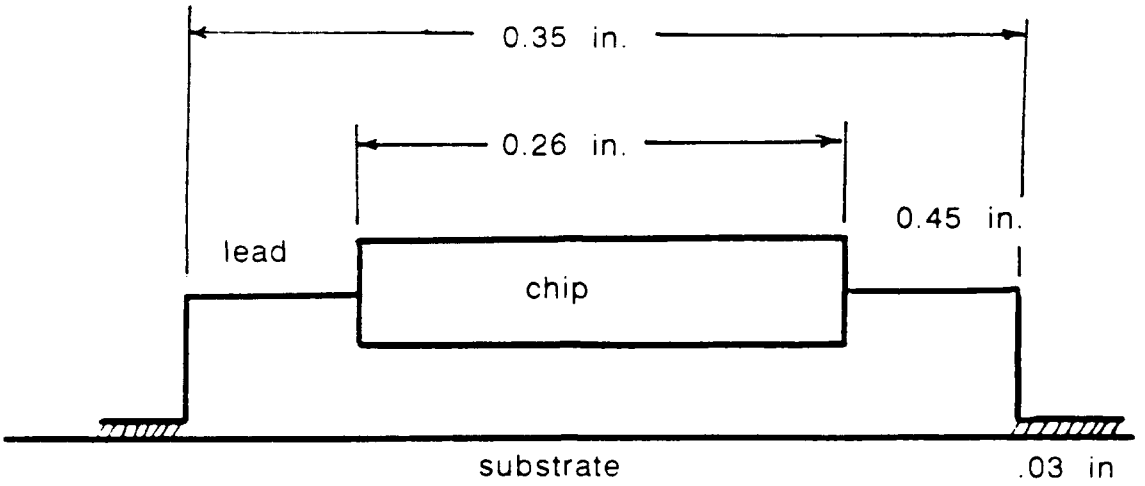

Figure 1. Geometry of leaded device

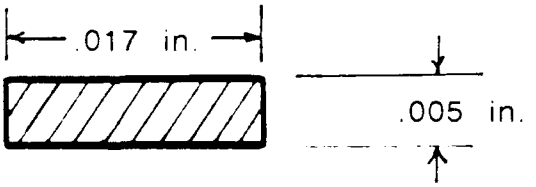

Figure 2. Cross section of lead wire

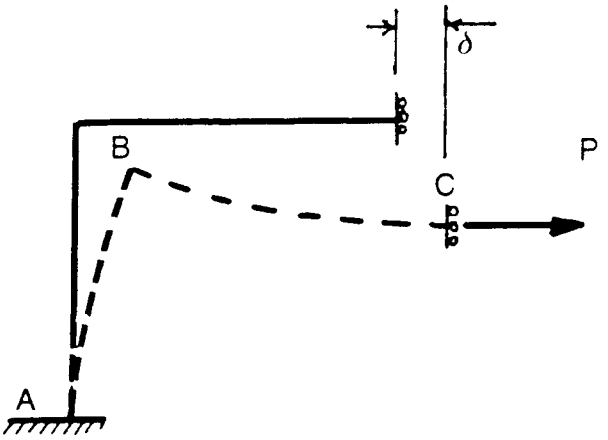

Figure 3. Support movement δ

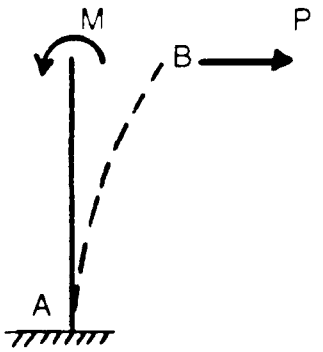

Figure 4. Deformation of beam AB

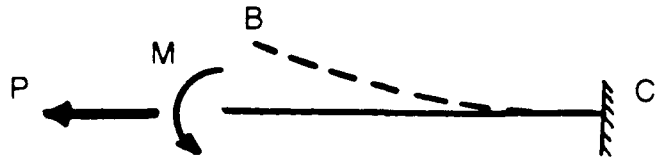

Figure 5. Deformation of beam BC

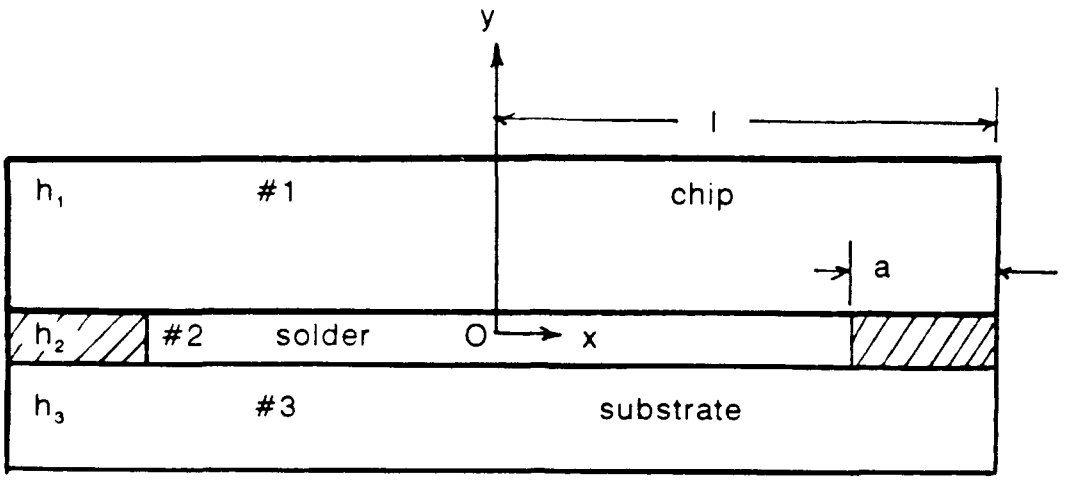

Figure 6. Unleaded device

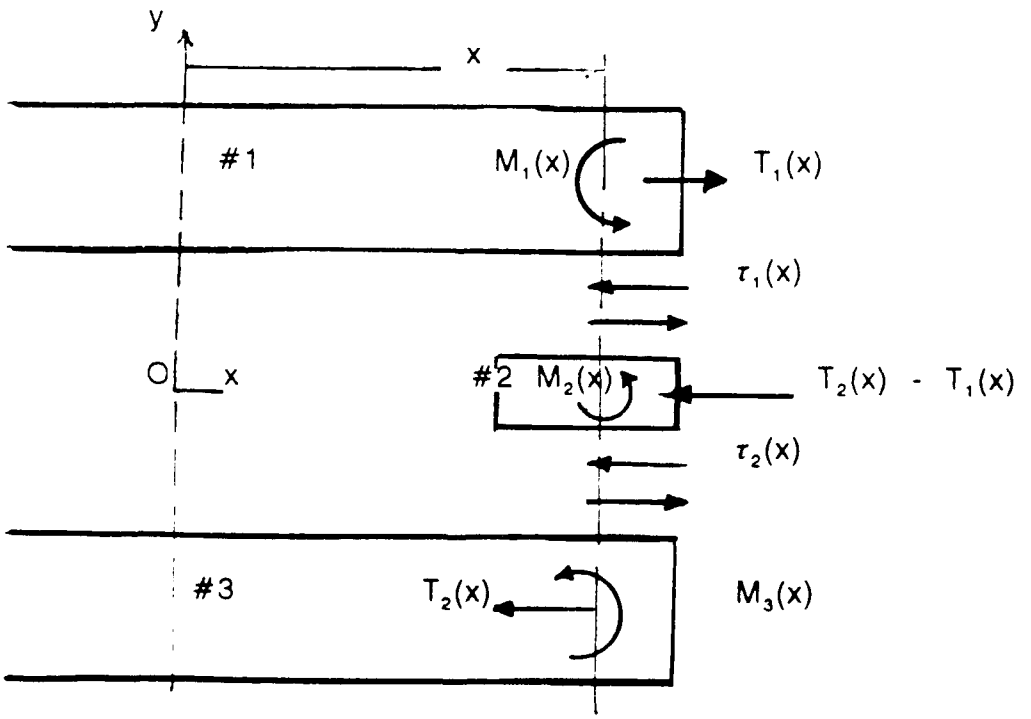

Figure 7. Force and moment equilibrium of components

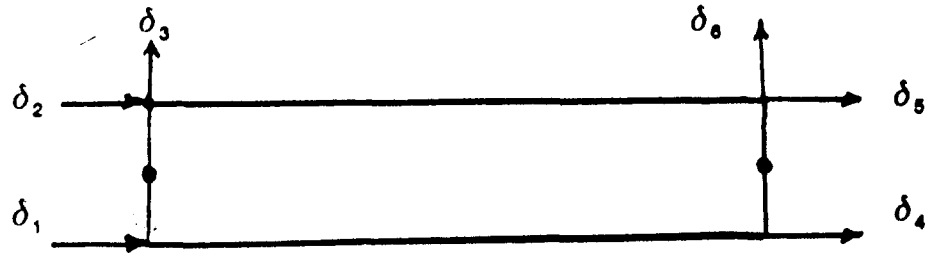

Figure 8. Six degree of freedom element

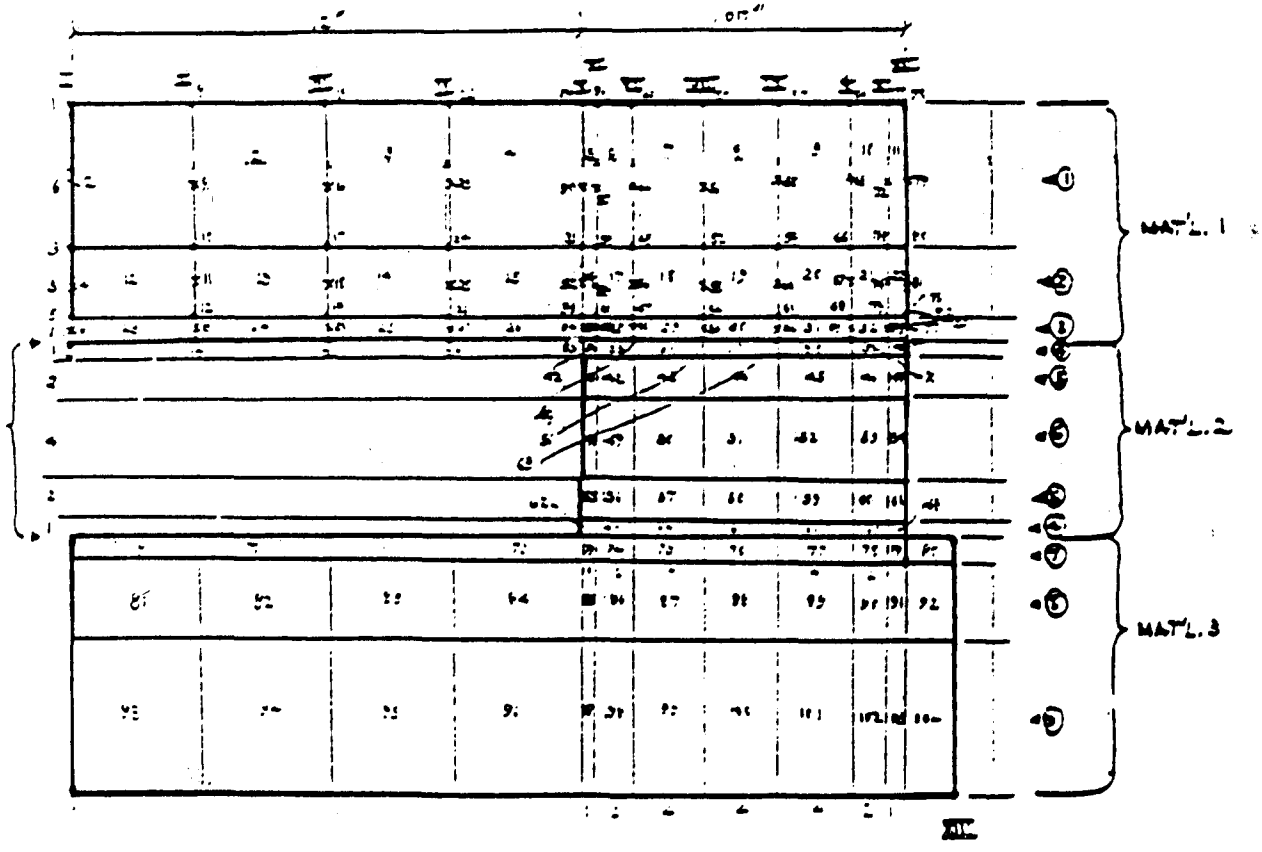

Figure 9. Finite element mesh

References

1. E. Suhir, 'Chapter 5, Thermal Stress Failures in Microelectronic Components - Review and Extension', pp.337-412, in Advances in Thermal Modeling of Electronic Components and Systems, Volume 1, edited by A. Bar-Cohen and A.D. Krauss, Hemisphere Publishing, Corp., New York, 1988.

2. D. Salinas and Y.W. Kwon, 'Thermoelastic Stresses in Multi-layered Media in a Non-uniform Temperature Field', submitted for presentation to the Pan American Congress of Applied Mechanics (PACAM III) to be held in Sao Paulo, Brazil, Jan 4-8, 1992.

DISTRIBUTION LIST

Office of Naval Research Director, Technology (Code 02) 800 North Quincy Street Arlington, VA 22217-5000	1 copy
Office of the Director of Defense Research and Engineering Information Office Library Branch The Pentagon, Rm. 3E 1006	1 copy
Defense Technical Information Center Cameron Station Alexanderia, VA 22314	2 copies
Naval Postgraduate School Technical Library (Code 52) Monterey, CA 93943-5100	2 copies
Research Administration (Code 81) Naval Postgraduate School Monterey, CA 93943-5100	1 copy
Professor A.J. Healey Dept. of Mech. Engn'g. Naval Postgraduate School Monterey, CA 93943-5100	1 copy
Prof. Young W. Kwon Dept. of Mech. Engng. Naval Postgraduate School Monterey, CA 93943-5100	1 copy
Commanding Officer Naval Weapons Support Center (Code 0211) Crane, Indiana 47522	3 copies
Prof. Young S. Shin Dept. of Mech. Engn'g. Naval Postgraduate School Monterey, CA 93943-5100	1 copy
Prof. Philip Y. Shin Dept. of Mech. Engn'g. Naval Postgraduate School Monterey, CA 93943-5100	5 copies
Prof. David Salinas Dept. of Mech. Engn'g. Naval Postgraduate School Monterey, CA 93943-5100	5 copies